Development of SIS Mixers for SMA 400-520 GHz Band

Chao-Te Li, Tse-Jun Chen, Tong-Liang Ni, Wei-Chun Lu, Chuang-Ping Chiu, Chong-Wen Chen, Yung-Chin Chang, Ming-Jye Wang and Sheng-Cai Shi

***Abstract*—SIS junction mixers were developed for SMA 400-520 GHz band. The results show receiver noise temperature around 100 K across the band, with noise contribution from RF loss and IF estimated to be around 50 K and 20K, respectively. Two schemes were used to tune out junction's parasitic capacitance. When a parallel inductor is employed, the input impedance is close to R_n, which facilitates impedance matching between the junction and the waveguide probe. Waveguide probes were designed to achieve a low feed-point impedance to match to the junction resistance. Optimum embedding impedances for lower receiver noise temperature were investigated. Performances of two schemes and composition of receiver noise were also discussed.**

***Index Terms*—integrated tuning circuit, SIS junction mixer, SMA, waveguide probe**

I. Introduction

The Sub-millimeter Array (SMA)[1,2], constructed by Smithsonian Astrophysical Observatory (SAO) and Institute of Astronomy and Astrophysics, Academia Sinica (ASIAA) is a radio interferometer of eight 6-m antennas. Receivers with superconducting-insulator-superconducting (SIS) mixers are being used for observations through major submillimeter atmospheric windows from 180 GHz to 900 GHz. This paper describes the development of SIS mixers for one target frequency band (400-520 GHz). The emphasis of this work is to compare mixer designs with two different tuning schemes and explore the optimum embedding impedance for lower receiver noise temperature. We adopted the single-junction design, considering low LO power available at high frequencies.

II. Waveguide Probe Design

To be consistent throughout the array operations, we adopted SAO's mixer block design. A detailed drawing of the center portion of the mixer block is shown in Fig. 1. The reduced height waveguide section (0.55 x 0.138 mm) has a fixed back-short, measuring 0.17 mm in depth. The fused quartz mixer chip, measuring 0.250 x 0.050 x 2.276 mm, is clamped between the horn section and the back piece of the block in a suspended microstrip configuration. The thickness of the substrate is reduced from 0.060 mm to 0.050 mm to avoid higher order modes of propagation along the microstrip transmission lines seen during simulations.

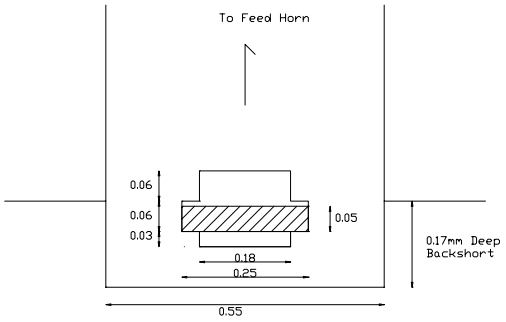

Fig. 1. Sectional view of the mixer block center portion. The quartz substrate is hatched. The cross section of the suspended microstrip and the fixed back-short of the block are shown. All dimensions are in mm.

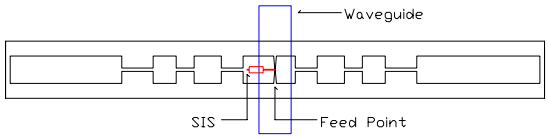

Fig. 2. Top view of the mixer chip sitting in a channel along the E-plane of the waveguide.

A bow-tie probe[3] was used with its feed point located at the center of the waveguide. The RF chokes following the low-impedance sections of the probe present an open at RF to the probe. The feed-point impedance can be reduced by shortening the lengths of probe's low-impedance sections. However, to accommodate the circuit consisting of the SIS junction, the tuning circuit, and impedance transformers, one side of the probe is extended as shown in Fig. 2. The shape of the probe also has some effect. In general, a broader probe (large θ in Fig. 5) yields a lower feed-point impedance. This configuration, along with the RF chokes, creates a feed-point impedance of about 26 Ω – j 23 Ω at 460 GHz, shown as the blue trace in Fig. 3. The waveguide probe was simulated using

C. T. Li, T. J. Chen, T. L. Ni, W. C. Lu, C. P. Chiu, C. W. Chen, Y. C. Chang and M. J. Wang are with the Institute of Astronomy and Astrophysics, Academia Sinica, Taipei, 10617 Taiwan (phone: 886-2-3365-2200; fax: 886-2-2367-7849; e-mail: ctli@asiaa.sinica.edu.tw).

S. C. Shi is with the Purple Mountain Observatory, Chinese Academy of Sciences, Nanjing, 210008 China (e-mail: scshi@mail.pmo.ac.cn).

a 3-D EM field simulator (HFSS). During simulations, the back-short depth was reduced to rotate the impedance locus onto the real axis of the Smith chart, shown as the red trace in Fig. 3.

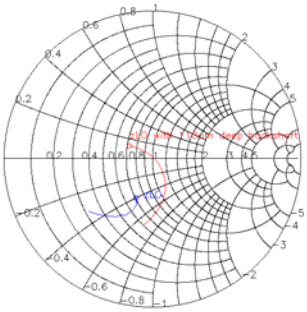

Fig. 3. Locus of the waveguide probe feed point impedance (in blue), and that with a reduced back-short (in red) from 400 GHz to 520 GHz. Circles mark where the impedances are at 400 GHz.

III. Tuning Circuits

There are two different schemes to tune out the junction's capacitance, as shown in Fig. 4, along with their corresponding optimum source resistance. End-loaded stubs were widely used as series inductors. This topology also lends itself to distributed junction designs. However, after the junction's capacitance is tuned out, the resistance converted by the series inductor is $R' = R/(\omega RC)^2$, much lower than R when $(\omega RC)^2 >> 1$. It usually requires 2 quarter-wavelength impedance transformers to bring the input impedance up to the level of few tens of ohms to match the feed-point impedance, as shown in Fig. 5. On the other hand, with a parallel inductor, the input impedance of the tuned junction is R, which is on the order of the junction normal state resistance R_n. Thereby only one or none impedance transformer is needed. This facilitates the impedance matching between the junction and the waveguide probe. Hopefully the bandwidth of the design would not be affected by that of transformers.

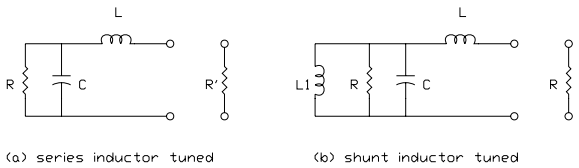

Fig. 4. Equivalent circuits of (a) a series inductor end-loaded with a junction, and (b) a parallel-inductor-tuned junction, where C represents the junction capacitance, R is the junction resistance, and $R' = R / (\omega RC)^2$.

For our designs, the end-loaded configuration corresponds to Fig. 1 (b) in [4] with $\omega RC \sim 4$ and $\omega L/R \sim 0.3$. The parallel-inductor-tuned case can be referred to Fig. 1 (c) in [4] with L = 0. From the analysis[4], despite the difference in input impedances, both configurations have similar bandwidths when terminated with their respective optimum source resistance. To increase the bandwidth, it would be necessary to reduce the value of ωRC or adopt a multi-junction design.

Fig. 6 shows how the input impedances at LO frequencies Z_{inLO} evolve after each section of transmission lines for our end-loaded design. Z_{inLO} is calculated via the complex current response of the junction at each LO frequency. The value could be quite different from the input impedance at RF, Z_{in}, which is derived from inversion of junction's admittance matrix. Simulation is done using the 5-port approximation to the quantum mixer theory[5] and an analytical model for thin-film superconducting microstrip lines[6]. The design comprises Nb/Al-AlO_x/Nb tunnel junctions integrated with Nb/SiO_2/Nb microstrip tuning circuits. The junction is characterized by a normal state resistance R_n of 19.5 Ω, J_c of 10 kA/cm^2, a junction area of 1 μm^2, and a junction capacitance of 90 fF. The simulated single-side-band (SSB) T_{RX} is shown in Fig. 7, along with the LO coupling and 4 times quantum noise limit.

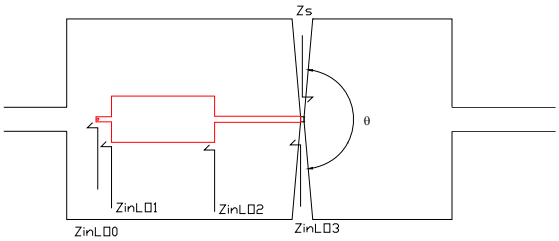

Fig. 5. The tuning circuit and impedance transformers for an end-loaded design, where $Z_{inLO\,i}$, i = 1, 2, and 3, is the input impedance of the junction after each section of transmission line at LO frequencies, and Z_s is the feed-point impedance.

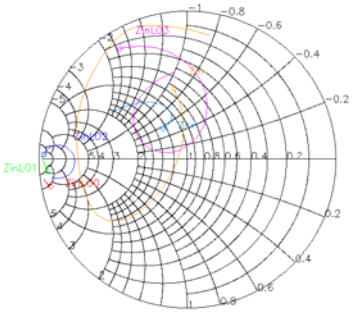

Fig. 6. Loci of the input impedance of the junction, Z_{inLO0} and those after each section of transmission line ($Z_{inLO\,i}$, i = 1, 2, and 3) of the end-loaded design at LO frequencies from 380 to 540 GHz. Z_{in} is the input impedance at signal frequencies. Z_s* is the complex conjugate of the feed point impedance. Circles indicate the start of impedance loci at 380 GHz. After the series inductor (or the end-loaded stub), the imaginary part of junction admittance is mostly cancelled, while the remaining resistance is on the order of 1 Ω. After 2 impedance transformers, the input impedance Z_{inLO3} is close to where Z_s* is on the Smith chart.

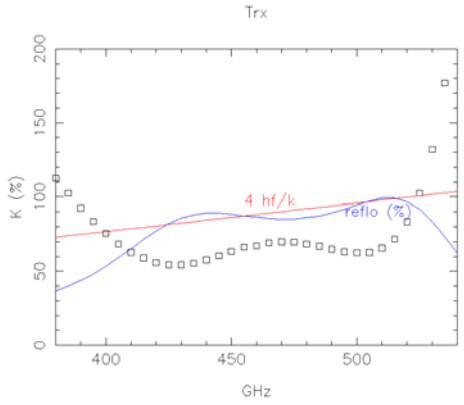

Fig. 7. The simulated SSB T_{RX} (square markers) of the series-inductor-tuned mixer design shown in Fig. 5. Four times quantum noise is plotted (red line) as a reference. The LO coupling (blue trace) is also shown. It is seen that good LO coupling corresponds to good T_{RX}, with a little displacement caused by the effects of G_m and T_{IF}.

In Fig. 8, for the design using a parallel inductor, a quarter-wavelength low-impedance open stub presents an RF short to a short, high-impedance stub as the inductor. The remaining resistance of the junction is about 18 Ω, close to the optimum resistance of 22 Ω derived from an empirical formula[7]

$$G_s = \frac{1}{2} + \frac{1}{4\omega}. \tag{1}$$

Since there is still some impedance difference, one transformer is placed between the junction and the feed-point. The impedance loci are shown in Fig. 9. The simulated T_{RX}, similar to that of the end-loaded design, is shown in Fig. 10.

IV. Optimum Embedding Impedance for Low Receiver Noise Temperature

To explore the optimum embedding impedance for lower receiver noise temperature, it is clear to look at the junction tuned with a parallel inductor so that the junction input impedance would not be transformed to a very small value after the inductor as in the end-loaded case. For the configuration in Fig. 7 without the transformer, Junction's capacitance is cancelled at LO of 485 GHz for our design. After calculations of the receiver noise temperature T_{RX}, the mixer noise temperature T_m, the mixer conversion gain G_m and the LO coupling over the Smith chart, as in Fig. 11, we can plot the contour enclosing the region where the T_{RX} is less than 70 K. Similarly, contours for T_m less than 40 K, G_m better than -2 dB, and LO coupling better than 95% can be drawn. Here

$$T_{RX} = T_m + \frac{T_{IF}}{G_m}. \tag{2}$$

All these values are for the single side band and the noise temperature of the IF chain T_{IF} is assumed to be 15 K. From Fig. 11, it can be seen that low T_{RX} can be achieved over a rather broad range on the Smith chart. The T_m contour does not coincide with the T_{RX} contour because the effects of T_{IF} and G_m.

On the other hand, the T_m contour is quite aligned with the LO coupling. Here the LO coupling is defined as the portion of available LO power delivered to the junction, namely

$$\frac{4\,\mathrm{Re}(Z_s)\,\mathrm{Re}(Z_{inLO})}{|Z_s + Z_{inLO}|^2}.$$

Since T_m is mainly due to correlation of the shot noise excited by the LO current[5], it is interesting to see that low T_m can be achieved when LO coupling is optimized.

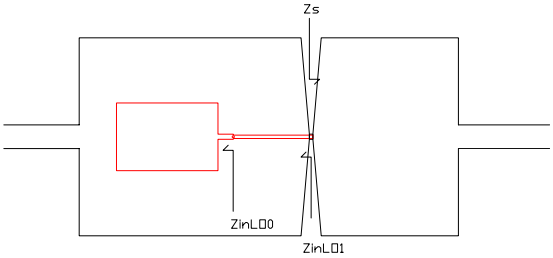

Fig. 8. Tuning circuit and impedance transformer for a SIS junction tuned with a parallel inductor.

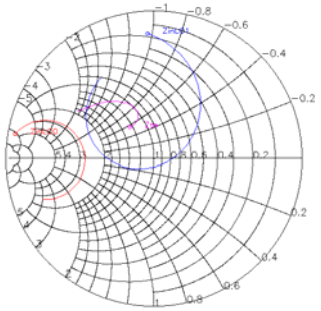

Fig. 9. Loci of the input impedance of the tuned junction Z_{inLO0} and that after the impedance transformer Z_{inLO1}, along with the complex conjugate of the feed point impedance Z_s* at LO frequencies from 380 to 540 GHz.

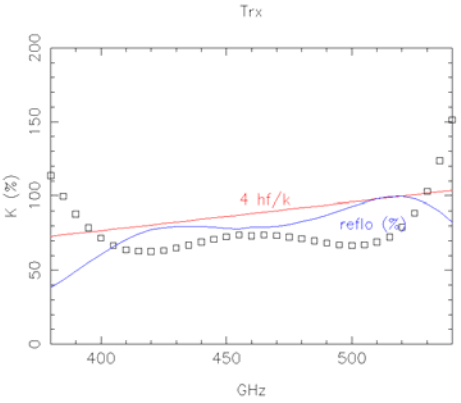

Fig. 10. The simulated SSB T_{RX} (squares), 4 times quantum noise limit (the red line), and the LO coupling (the blue trace) for the parallel-inductor-tuned mixer design shown in Fig. 8.

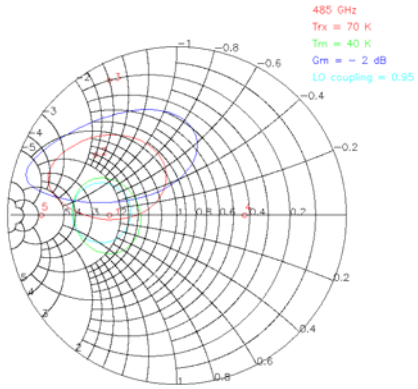

Fig. 11. Contours of T_{RX} (red), T_m (green), G_m (blue), and LO coupling (cyan) on the Smith chart for the design with a parallel inductor tuning circuit at 485 GHz, where junction's parasitic capacitance is cancelled. The optimum source conductance to give better T_m is around 2.5 (normalized to 1/50 Ω^{-1}), which corresponds to a source resistance of 20 Ω, consistent with the value given by (1).

V. Testing

A. *Parallel-inductor- tuned*

From receiver noise temperature measurements using the standard hot/cold load technique, some samples with a parallel inductor show a bandwidth not as wide as designed, as shown in Fig. 12. There are 2 factors that might cause this discrepancy. One possibility is the low R_n seen in these devices. Another factor might be the frequency response of the open stub used as a short to the parallel inductor. The bandwidth of a 1/4 wavelength open stub might be narrower, compared to a radial open stub. In addition, the discontinuity (the abrupt width change) between the open stub and the inductor is not modeled yet during simulation. There is an intention to have some designs using radial stubs for further verification.

We also did some analysis to break-down each contribution to the receiver noise temperature at several LO frequencies from the measurements of one device (460NTHU-1-1 IAA-C2-063) as shown in Table I.

TABLE I Receiver Noise Temperature Decomposition

LO Freq (GHz)	T_{RX} (K)	T_{RF} (K)	$T_{RF} + T_m/G_{RF}$ (K)	T_{IF} (K)	$G_{RF}\,G_m$ (dB)	T_{RX}' (K)
432	94.7	30.8	60.1	8.9	-3.9	82.2
452	126.7	35.3	90.9	8.9	-5.4	121.6
464	134.7	43.2	97.6	9.0	-5.4	128.7
488	126.7	49.9	94.9	9.2	-4.3	119.4

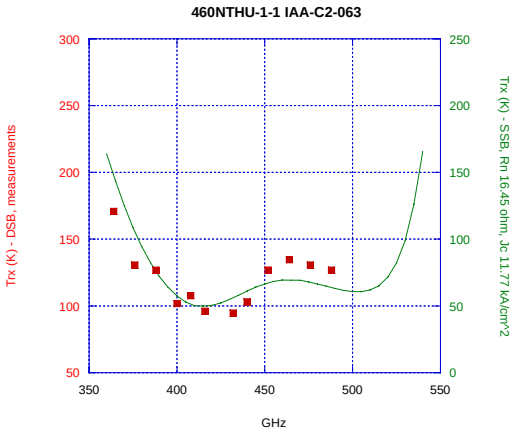

Fig. 12. Measured and simulated T_{RX} as a function of LO frequencies. The square is the double-side-band (DSB) T_{RX} measured from a sample (460NTHU-1-1 IAA-C2-063) with a parallel inductor, R_n = 16.5 Ω (lower than the design value of 19.5 Ω) and Jc = 11.8 kA/cm^2. The green trace is the simulated SSB T_{RX} from the design with the same junction parameters as the sample. Simulation results imply that besides the low R_n, there might be other factor responsible for the narrower bandwidth.

In Table I, at each LO frequency, T_{RX} is the measured DSB noise temperature. As shown in Fig. 13, T_{RX} can be decomposed into 3 terms, namely T_{RF} from the optical loss, T_m from the mixer itself, and T_{IF} from the IF amplifier, associated with the optical loss $1/G_{RF}$, and the mixer conversion gain G_m. The noise contribution from the optical loss T_{RF} is estimated using the intersecting-line method[8, 9]. T_{IF} is extrapolated along with the shot noise[10] of the junction above the gap voltage. Through this procedure, the correspondence between the noise temperature at mixer output and the measured IF power is established, from which we can figure out the overall conversion gain, i.e. $G_{RF}G_m$ of the system from the hot/cold load data. At last, $T_{RF} + T_m/G_{RF}$ can be estimated from the Y factor method with a modified Y factor as

$$Y' = \frac{P_{hot} - P_{gap}}{P_{cold} - P_{gap}} = \frac{T_{hot} + T_{RF} + T_m / G_{RF}}{T_{cold} + T_{RF} + T_m / G_{RF}}, \quad (1)$$

where P_{gap} is the IF power measured as the junction is biased at the gap voltage where the mixer conversion gain G_m can be considered as zero and the IF power output is due to T_{IF} alone[11]. The last column T_{RX}' is the sum of $T_{RF}+T_m/G_{RF}$ and $T_{IF}/(G_{RF}G_m)$. We can see that there are about 6 – 13 K discrepancy between the measured T_{RX} and the added-up one.

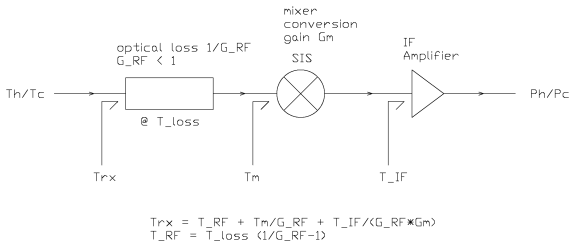

Fig. 13. Break-down of a receiver noise temperature (T_{RX}).

Using $T_{m,DSB}$ from simulations, we can further process the data to estimate G_{RF}, $G_{m,DSB}$, and T_{loss}, and compare with the $G_{m,SSB}$ from simulations for consistency check, as shown in Table II. At 432 and 488 GHz, $G_{m,DSB}$ agrees well with $G_{m,SSB}$ as $G_{m,DSB} = G_{m,SSB} + 3$ dB. The optical loss includes the loss (~ 0.07 dB) through the 5° LO coupling wire grid, the vacuum window, the IR blocking filter, the Teflon lens in front of the mixer block, and waveguide loss inside the mixer block. This might explain the low T_{loss} derived since the mixer block is anchored to 4 K.

TABLE II G_{RF}, $G_{m,DSB}$, AND T_{loss} DERIVED USING $T_{m,DSB}$ FROM SIMULATIONS

LO Freq (GHz)	$T_{m,DSB}$ (K)	T_m/G_{RF} (K)	G_{RF} (dB)	$G_{m,DSB}$ (dB)	$G_{m,SSB}$ (dB)	T_{loss} (K)
432	19.1	29.3	-1.9	-2.1	-4.8	57.2
452	21.0	54.7	-4.2	-1.2	-6.0	22.0
464	23.5	54.4	-3.7	-1.8	-5.9	32.9
488	26.3	45.0	-2.3	-1.9	-5.1	69.9

For direct detection, the sample was used as the detector in a Fourier transform Spectrometer (FTS). The results show that the device has reasonable response within the designed frequency range as shown in Fig. 14. One major factor that affects the FTS response is the product of the intrinsic current responsivity R_i of the junction to the radiation and the (LO) coupling, as plotted as the green trace in Fig. 15. As both T_{RX} and FTS response closely related to the (LO) coupling, proximity of low T_{RX} and the peak of the FTS response is observed.

For a sample with higher R_n (18.8 Ω, closer to the design value of 19.5 Ω), the frequency response has a wider bandwidth and agrees well with the simulation, except at higher frequencies near 500 GHz, as shown in Fig. 16. Limited by the LO available above 500 GHz at the moment, further tests above 500 GHz are required to verify the rising T_{RX} near 500 GHz.

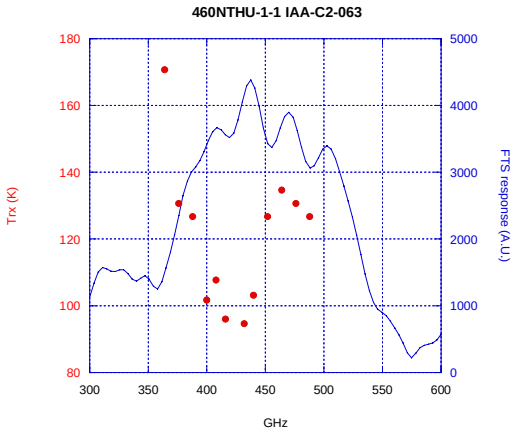

Fig. 14. T_{RX} as a function of LO frequencies and the measured FTS response. The lowest T_{RX} is close to where the peak FTS response is, with few GHz offset. Radiation intensity from the FTS is not yet calibrated.

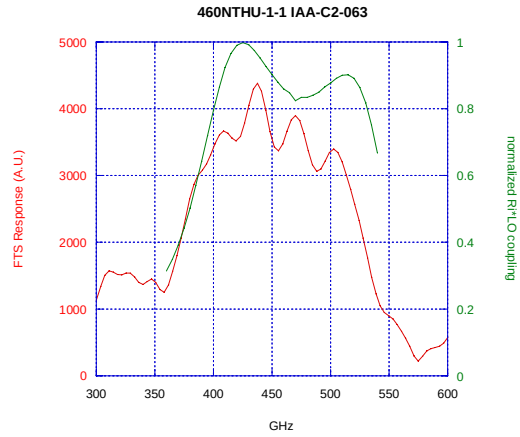

Fig. 15. The measured FTS response (red) and the simulation (the green trace as the product of the junction intrinsic current responsivity to LO - R_i and the LO coupling, normalized to its peak value). From simulation, R_i decreases monotonically to 65% from 360 GHz to 540 GHz while the LO coupling exhibits the 2-hump structure.

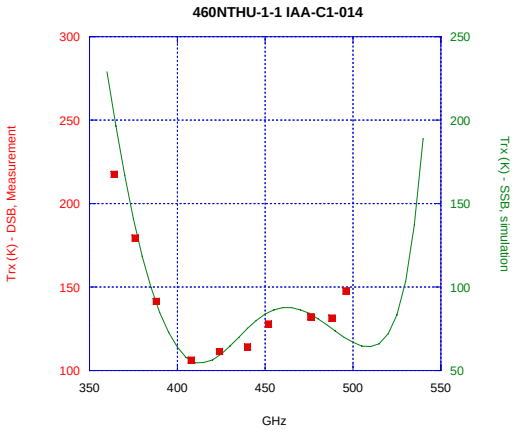

Fig. 16. Measured DSB T_{RX} of a device (460NTHU-1-1 IAA-C1-014) with a higher R_n (18.8 Ω, closer to the design value of 19.5 Ω) and simulations as a function of LO frequencies. The squares are the measured DSB T_{RX}. The green curve is the simulated SSB T_{RX} from the same design with R_n = 19.5 Ω, junction area of 1 μm^2 and junction capacitance of 90 fF. The measurements were done with 10° LO wire grid (94% transmission) and a un-blazed Teflon lens in front of the mixer block. As a result, the noise contribution from the optical loss (T_{RF}) is between 60 - 70K.

B. End-loaded scheme

For devices with an end-loaded inductive stub, despite the 2 quarter wavelength transformers used to transform the low impedance (< 1 Ω) of the tuned junction to the level of the embedding impedance, the test results show this kind of design exhibits a comparable bandwidth, as shown in Fig. 17 and 18. Similar noise analysis is done for one device (460NTHU-1-1 IAA-C5-047), listed in Table III. The difference between the measured T_{RX} and the added-up one is now less than 10 K.

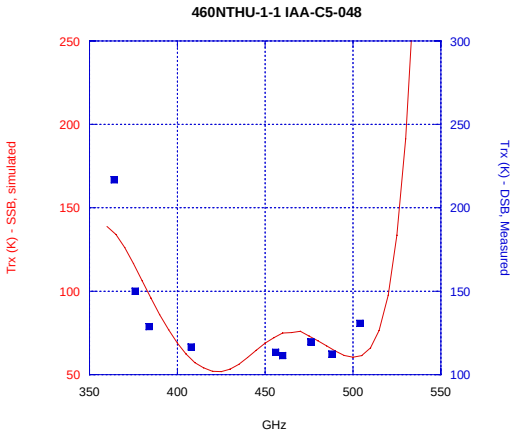

Fig. 17. T_{RX} of a device (460NTHU-1-1 IAA-C 5-048) with an end-loaded tuning stub as a function of LO frequency. The blue squares are measured DSB T_{RX}, while the red trace represents the simulated SSB T_{RX} with the same junction normal state resistance R_n, junction area, and the super current density J_c as the sample. The measurements follow the simulation quite well, except at 1 or 2 data points. During the testing, the noise contribution from the IF amplifier T_{IF} is estimated to be around 17K. The noise due to optical loss T_{RF} is estimated to be from 66 to 77K. T_{RF} is rather large because of the large degrees of LO coupling wire grid (10°, corresponding to 94% transmission) and a Teflon lens without anti-reflection blazing used in front of the mixer block.

VI. Conclusion

SIS junction mixers with 2 different tuning schemes were designed and tested for SMA 400-520 GHz band. The design with a parallel inductor has the advantage of higher input resistance. Thereby the matching between the junction and the probe can be and more compact and less complicated. However, from both simulations and measurements, two schemes have similar performances, with regard to receiver noise temperature or bandwidth. The optimum embedding impedance for low mixer noise temperature T_m is found to be where the LO coupling is efficient. Further testing is required to verify the mixer response above 500 GHz, as well as the effect of the open stub in the parallel-inductor-tuned design.

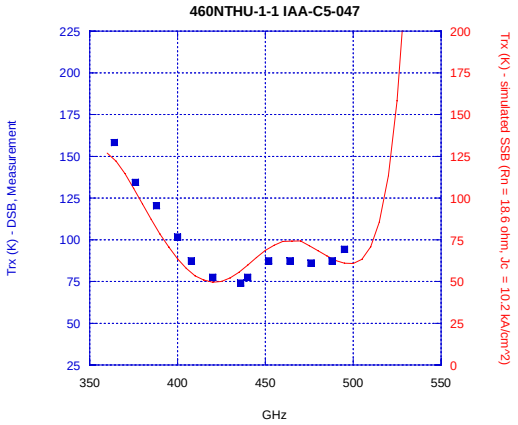

Fig. 18. Measured and simulated T_{RX} of another device (460NTHU-1-1 IAA-C5-047) also with an end-loaded tuning stub as a function of LO frequency. The blue squares are measured DSB T_{RX}, while the red trace represents the simulated SSB T_{RX} with the same junction normal state resistance R_n, junction area, and the super current density J_c as the sample. During the test, a smaller LO wire grid angle (5°, corresponding to 98.5% transmission, except at 495 GHz, where the wire grid is 10°) and a Teflon lens with anti-reflection blazing were used. Break-down of receiver noise contribution is listed in Table III.

TABLE III Receiver Noise Temperature Decomposition

LO Freq (GHz)	T_{RX} (K)	T_{RF} (K)	$T_{RF} + T_m/G_{RF}$ (K)	T_{IF} (K)	$G_{RF}\ G_m$ (dB)	T_{RX}' (K)
436	79.8	49.8	67.2	7.7	-2.5	80.9
452	93.3	52.7	70.0	7.6	-2.7	84.1
464	93.3	50.6	69.1	7.5	-3.1	84.4
488	93.3	57.6	75.6	7.9	-2.0	88.2

References

[1] R. Blundell, C. E. Tong, D. C. Papa, R. L. Leombruno, X. Zhang, S. Paine, J. A. Stern, H. G. LeDuc, and B. Bumble, "A wideband fixed-tuned SIS receiver for 200-GHz Operation," *IEEE Trans. Microwave Theory Tech.*, vol. 43, pp. 933-937, 1995.

[2] C. E. Tong, R. Blundell, S. Paine, D. C. Papa, J. Kawamura, X. Zhang, J. A. Stern, and H. G. LeDuc, "Design and characterization of a 250-350 GHz fixed-tuned superconductor-Insulator-superconductor receiver," *IEEE Trans. Microwave Theory Tech.*, vol. 44, pp. 1548-1556, 1996.

[3] A. V. Raisanen, W. R. McGrath, D. G. Crete, and P. L. Richards, "Scaled model measurements of embedding impedances for SIS waveguide mixers," *Int. J. IR and MM Waves*, vol. 6, pp. 1169-1189, 1985.

[4] A. R. Kerr, "Some fundamental and practical limits on broadband matching to capacitive devices, and the implications for SIS mixer design," *IEEE Trans. Microwave Theory Tech.*, vol. 43, pp.2-13, 1995.

[5] J. R. Tucker, "Quantum limited detection in tunnel junction mixers," *IEEE Journal of Quantum Electronics*, vol. QE-15, pp.1234-1258, 1979.

[6] W. H. Chang, "The inductance of a superconducting strip transmission line," *J. Appl. Phys.*, vol. 50, pp.8129-8134, 1979.

[7] Q. Ke, M. J. Feldman, "Optimum source conductance for high frequency superconducting quasiparticle receivers," *IEEE Trans. Microwave Theory Tech.*, vol. 41, pp.600-604, 1993.

[8] R. Blundell, R. E. Miller, and K. H. Gundlach, "Understanding Noise in SIS Receivers," *Int. J. IR and MM Waves*, Vol. 13, No. 1, pp. 3-26, 1992.

[9] Q. Ke and M. J. Feldman, "A technique for noise measurements of SIS receivers," *IEEE Trans. Microwave Theory Tech.*, 42, 752, 1994.

[10] D. P. Woody, R. E. Miller, and M. J. Wengler, "85-115 GHz receivers for radio astronomy," *IEEE Trans. Microwave Theory Tech.*, 33, 90, 1985.

[11] S. C. Shi, "Quantum-limited broadband mixers with superconducting tunnel junctions at millimeter and submillimeter wavelengths," Ph.D. Dissertation, 1996